

# 1 Understanding the Drying Behavior of 2 Regenerated Cellulose Gel Beads: The Effects of 3 Concentration and Non-solvents

4 Hailong Li<sup>1,2\*</sup>, Margarita Kruteva<sup>3</sup>, Martin Dulle<sup>3</sup>, Zhen Wang<sup>1</sup>, Katarzyna Mystek<sup>1</sup>,  
5 Wenhai Ji<sup>4</sup>, Torbjörn Pettersson<sup>1,5\*</sup>, and Lars Wågberg<sup>1,5\*</sup>

6  
7 <sup>1</sup>Department of Fibre and Polymer Technology, KTH Royal Institute of Technology, Teknikringen  
8 58, SE-100 44 Stockholm, Sweden

9 <sup>2</sup>Department of Physics, AlbaNova University Center, Stockholm University, 10691 Stockholm,  
10 Sweden

11 <sup>3</sup>Jülich Centre for Neutron Scattering and Biological Matter (JCNS-1/IBI-8), Forschungszentrum  
12 Jülich GmbH, Wilhelm-Johnen-Straße, D-52425 Jülich, Germany

13 <sup>4</sup>Deutsches Elektronen-Synchrotron (DESY), Notkestr. 85, 22607 Hamburg, Germany

14 <sup>5</sup>Wallenberg Wood Science Centre, Department of Fibre and Polymer Technology, KTH Royal  
15 Institute of Technology, Teknikringen 56, 10044 Stockholm, Sweden

16

17 **ABSTRACT:** The drying behavior of regenerated cellulose gel beads swollen with different  
18 non-solvents (*e.g.*, water, ethanol, water/ethanol mixtures) is studied *in situ* on the macroscopic  
19 scale with an optical microscope, as well as on nano-scale using Small-Angle/Wide-Angle X-ray  
20 Scattering (SAXS/WAXS) techniques. Depending on the cellulose concentration, the structural  
21 evolution of beads during drying follows one of three distinct regimes. Firstly, when the cellulose  
22 concentration is lower than 0.5 wt%, the drying process comprises three steps and, regardless of

1 the water/ethanol mixture composition, a sharp structural transition corresponding to the formation  
2 of a cellulose II crystalline structure is observed. Secondly, when the cellulose concentration is  
3 higher than 5.0 wt%, a two-step drying process is observed and no structural transition occurs for  
4 any of the beads studied. Thirdly, when the cellulose concentration is between 0.5 and 5.0 wt%,  
5 the drying process is dependent on the non-solvent composition. A three-step drying process takes  
6 place for beads swollen with water/ethanol mixtures with a water content higher than 20%, while  
7 a two-step drying process is observed when the water content is lower than 20%. To describe the  
8 drying behavior governed by the cellulose concentration and non-solvent composition, a simplified  
9 phase diagram is proposed.

10 **KEYWORDS:** regenerated cellulose, gel bead, drying kinetics, non-solvent, cellulose  
11 concentration

## 13 INTRODUCTION

14 Cellulose is one of the most abundant natural polymers on earth and has been used in a variety of  
15 applications due to its excellent physical, mechanical, and biocompatible properties.<sup>1-3</sup> High-  
16 performance products, such as high tenacity rayon,<sup>4,5</sup> transparent films,<sup>6-8</sup> hydrogels and  
17 aerogels,<sup>9-11</sup> as well as spheres and beads<sup>12</sup> can be fabricated by the regeneration of cellulose  
18 solutions into materials that can be used in dry state where they exhibit good strength and  
19 toughness. The mechanism of cellulose dissolution has been intensively studied using several  
20 different solvent systems, notably mixtures of lithium chloride and *N,N*-dimethylacetamide  
21 (LiCl/DMAc)<sup>13-19</sup> which is used in this work. However, a limited number of studies have  
22 investigated the kinetics of the microstructural evolution during the drying of regenerated  
23 cellulose.<sup>20</sup> This is a crucial step in shaping cellulose materials from the wet state, it is essential to

1 determine how the micro- or nanoscale structures change during the removal of water or other  
2 regenerating solvents. To simplify these studies, it is important to prepare well-defined model  
3 systems for the cellulose-based materials. It has already been shown that cellulose gel beads, which  
4 are smooth on the nanoscale and can be prepared by precipitating the cellulose solution into a non-  
5 solvent (ethanol or water), can be used as a suitable model system.<sup>21-26</sup> This is mostly due to the  
6 fact that it has been possible to accurately characterize the highly homogeneous structure of  
7 cellulose beads and show that they are composed of a non-crystalline, molecularly dispersed  
8 cellulose network.<sup>22,23</sup> Such systems have already been used to investigate the swelling behavior  
9 of wet, delignified cellulosic wood fibres;<sup>22,23</sup> the adhesion of two cellulose surfaces;<sup>21,26</sup> and the  
10 influence of polymer grafting on the adhesion of modified beads on a molecular scale.<sup>24</sup> However,  
11 the structural development during drying from different solvents, and for different starting  
12 concentrations of the cellulose solution are still unexplored research areas.

13 X-ray scattering is a powerful technique, used to investigate the micro structure of almost every  
14 kind of material, including cellulose.<sup>27</sup> For example, Grazing Incidence Small-Angle X-ray  
15 Scattering (GISAXS) has been used to investigate supramolecular rearrangements in cellulose thin  
16 films during the conversion of trimethylsilyl cellulose to cellulose *via* HCl vapor hydrolysis.<sup>28,29</sup>  
17 GISAXS was also employed by Roth *et al.* to characterize the structure of spray-deposited  
18 nanocellulose thin films and water-induced structural rearrangements during drying.<sup>30,31</sup> In our  
19 previous work, Small-Angle and Wide-Angle X-ray Scattering (SAXS and WAXS) methods were  
20 utilized to trace the structural evolution of 1.5 wt% regenerated cellulose gel beads (swollen in  
21 water or ethanol) during drying.<sup>25</sup> Likewise GISAXS in combination with AFM was used to trace  
22 the structural evolution of cellulose-cellulose interfaces joining together during drying.<sup>26</sup> In the  
23 present work, the objective was to explore how the cellulose gel beads dry when different cellulose

1 concentrations and non-solvent compositions are used. Consequently, a comprehensive evaluation  
2 of the microstructural changes of cellulose gel beads clarifies how cellulose surfaces consolidate  
3 during the drying of cellulose-rich materials.

4 In this study, cellulose gel beads were prepared using different cellulose concentrations and  
5 swollen by different non-solvents: water, ethanol, and water/ethanol mixtures; as depicted in  
6 **Figure 1a**. The change in diameter of the beads was recorded with an optical microscope during  
7 drying (Figure 1b). The micro- or nanoscale structural evolution during drying was investigated  
8 using *in situ* SAXS and WAXS techniques. Additionally, the drying behavior of cellulose gel  
9 beads is discussed and illustrated in a simplified phase diagram.

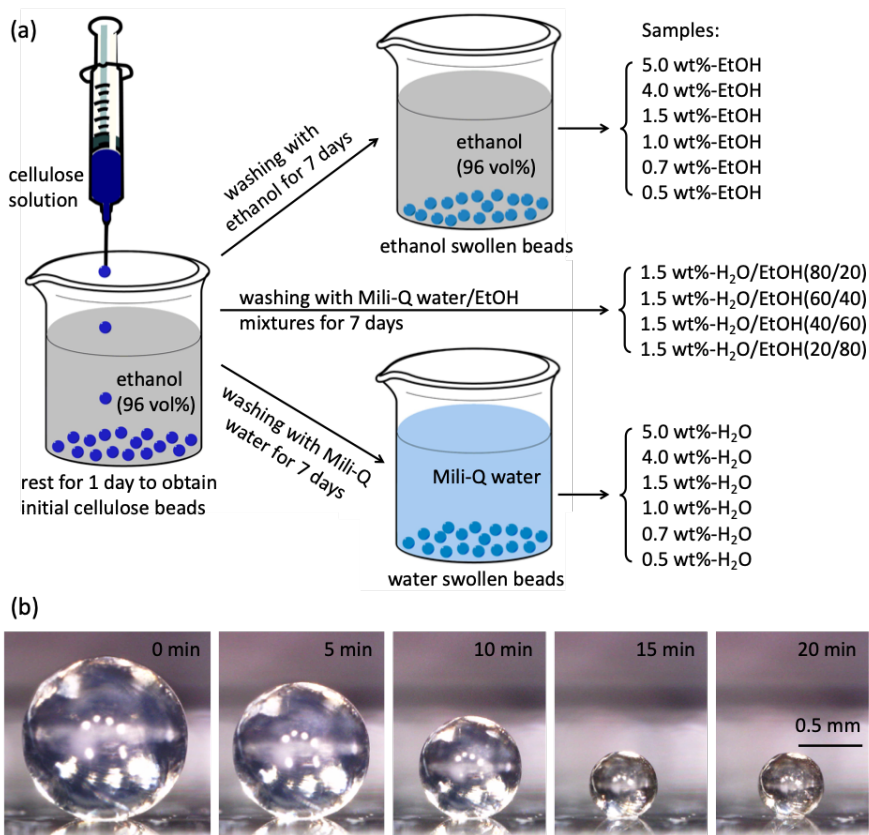


**Figure 1.** (a) Schematic illustration of the preparation of the cellulose gel beads swollen in water, ethanol, and water/ethanol mixtures. All the samples are listed in the panel on the right-hand side. (b) Side-view optical microscope images of cellulose gel bead (1.5 wt%-H<sub>2</sub>O) during drying on a glass slide at 22 °C and 28% RH. The scale bar corresponds to a length of 0.5 mm for all the images.

## RESULTS AND DISCUSSION

**Interior morphologies of the initial cellulose gel beads.** The scanning electron microscopic (SEM) images of the internal structure of Critical Point Dried (CPD) ethanol swollen beads are

1 shown in **Figure 2**. A porous 3D network composed of fibrillar cellulose is observed for all types  
2 of CPD beads. This porous structure is more obvious for the low cellulose concentration beads,  
3 such as the 0.5 and 0.7 wt% beads (Figure 2a' and 2b'). As the cellulose concentration increases  
4 the porous structure becomes denser, since the cellulose fibrils are thicker which causes a decrease  
5 in pore size (Figure 2a-2d, 2a'-2d'). When the cellulose concentration is 4 wt% or higher, the  
6 fibrillar networks are more compact, resulting in the pores becoming smaller and harder to observe  
7 (Figure 2e-2f and 2e'-2f'). Similar porous structure is observed from the SEM images of the  
8 interior of CPD dried water swollen beads (Figure S1), and the trend is consistent with ethanol  
9 swollen beads. For 1.5 wt% cellulose gel beads swollen by different water/ethanol mixtures, the  
10 porous structure becomes slightly denser when the water content in the water/ethanol mixture  
11 increases (Figure S2). It is expected to be caused by the large interaction between water and  
12 cellulose.

hat formatiert: Schriftart: Fett

hat formatiert: Schriftart: Fett

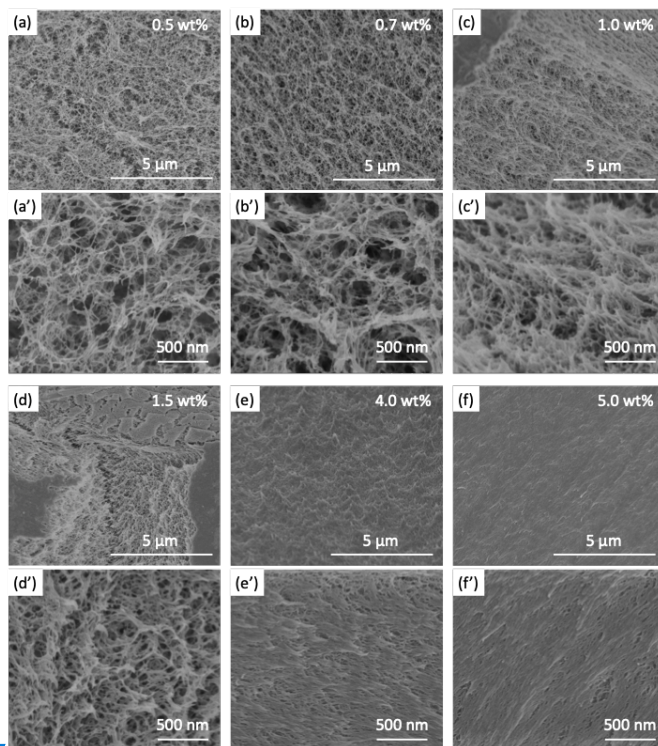


**Figure 2.** SEM images of the interior of CPD dried ethanol swollen cellulose beads prepared using different cellulose concentrations: (a, a') 0.5 wt%-EtOH, (b, b') 0.7 wt%-EtOH, (c, c') 1.0 wt%-EtOH, (d, d') 1.5 wt%-EtOH, (e, e') 4.0 wt%-EtOH, and (f, f') 5.0 wt%-EtOH. (a-g) are lower magnification SEM images and (a'-g') are higher magnification SEM images.

#### **Drying behavior of cellulose gel beads: microscopy.**

From the side-view optical microscope images captured during drying of a cellulose gel bead (Figure 1b), it can be seen that the swollen bead shrinks continuously and uniformly, retaining its spherical shape during the drying process.

This is consistent with our previous work.<sup>25,32</sup> Moreover, apart from the size decrease, the

transparency of the gel beads changes with evaporation, as shown in **Figure 3a and 3b**. For the

water swollen bead (1.0 wt%-H<sub>2</sub>O, in Figure 3a), the outer part becomes translucent during the

first 7 min, and then becomes more transparent for the following 14 min. After that, the entire bead

hat gelöscht:

1 remains transparent, up to and including when it is completely dry. The same phenomenon is  
2 observed for water swollen beads formed using other cellulose concentrations (**Figure S3**). In  
3 contrast, in the case of the ethanol swollen beads (1.0 wt%-EtOH, in Figure 3b), the outer part  
4 becomes opaque in the first 5 min and the bead never recovers its transparency, remaining opaque  
5 and grey when dried for 30 min. This phenomenon is also observed in other studies of ethanol  
6 swollen beads formed with different cellulose concentrations (**Figure S4**). This is most likely due  
7 to the multi-scattering and reflection of light inside the ethanol swollen beads; which have a  
8 tendency to keep their porous internal structure during drying, as established in our previous  
9 work.<sup>25</sup> For the water swollen beads, the fibrillar like structure in the drying bead is compacted  
10 and the light scattering pores, initially present during drying, are removed to such an extent that a  
11 transparent dry bead is formed. Schematic figures are provided on the right of Figure 3a and 3b to  
12 illustrate this.

13 Figure 3c and 3d show the diameter changes of the water swollen and ethanol swollen beads  
14 during the drying process, respectively, where the  $D/D_0$  values are the diameter of the bead ( $D$ )  
15 normalized to the initial diameter ( $D_0$ ). For the water swollen beads,  $D/D_0$  decreases linearly at  
16 short evaporation times (stage I, grey regime in Figure 3c); and the linear shrinking rate ( $k_1$ )  
17 decreases with the cellulose concentration after being relatively constant for the two lowest  
18 concentrations. After the first stage of drying, a fast linear shrinking with a higher rate,  $k_2$ , occurs,  
19 indicating that the drying stage II has begun (green regime in Figure 3c). This faster shrinking is  
20 more pronounced for low cellulose concentration gel beads, which have a shorter residence time  
21 in stage I drying. After drying for a certain time,  $D/D_0$  starts to become constant (red regime in  
22 Figure 3c) which is defined as the “equilibrated  $D/D_0$ ”. The ethanol swollen beads exhibit a  
23 different drying behavior, where only one linear shrinking phase is observed (Figure 3d) before



1 reaching the equilibrated  $D/D_0$ . These results support the proposed hypothesis that the light  
2 scattering pores, which are initially present in the internal structure of gel beads, are shrinking for  
3 water swollen beads, but are retained throughout the drying process of ethanol swollen beads. The  
4 reasons for this are discussed in more detail below with the results of the SAXS experiments.

5 Figure 3e summarizes the linear shrinking rate ( $k_1$  and  $k_2$ ) in the drying stages I and II vs.  
6 cellulose concentration for water swollen and ethanol swollen beads. For water swollen beads,  
7 with the exception of the 0.5 wt%-H<sub>2</sub>O bead, both  $k_1$  and  $k_2$  decrease with increasing cellulose  
8 concentration. The rate difference between  $k_2$  and  $k_1$  is reduced for samples with higher cellulose  
9 concentrations. For the 5 wt%-H<sub>2</sub>O beads,  $k_2$  is almost the same as  $k_1$ , which means that the faster  
10 shrinking during drying stage II is not as pronounced as with the lower concentration cellulose  
11 beads. In the case of ethanol swollen beads, it is observed that  $k_1$  decreases with increasing  
12 cellulose concentration. Furthermore, the values of  $k_1$  are significantly larger for the ethanol  
13 swollen beads than the  $k_1$  values of water swollen beads with the same cellulose concentration,  
14 which is most likely due to the faster evaporation rate of ethanol (due to its lower vapor pressure)  
15 at ambient conditions.

16 Figure 3f shows the change in equilibrated  $D/D_0$  vs. cellulose concentration for water swollen  
17 and ethanol swollen beads. It can be seen that the  $D/D_0$  value increases with higher cellulose  
18 concentrations for both water swollen and ethanol swollen beads; indicating that higher cellulose  
19 concentrations better preserve the initial bead size. Interestingly, for cellulose concentrations lower  
20 than or equal to 1.5 wt%, the equilibrated  $D/D_0$  values of ethanol swollen beads are smaller than  
21 those for the corresponding water swollen beads. This would suggest that these ethanol swollen  
22 beads shrink more than their water swollen bead counterparts. However, when higher cellulose  
23 concentrations are used (4.0 and 5.0 wt%), the equilibrated  $D/D_0$  values determined for ethanol

swollen beads are higher than those of the corresponding water swollen beads, meaning that the ethanol swollen beads shrink less. This phenomenon, together with the aforementioned slower shrinking rate ( $k_1$ ) for the 0.5 wt%-H<sub>2</sub>O bead, are linked to the micro-scale structural evolution of beads during drying from different solvents (discussed further in the WAXS section below).

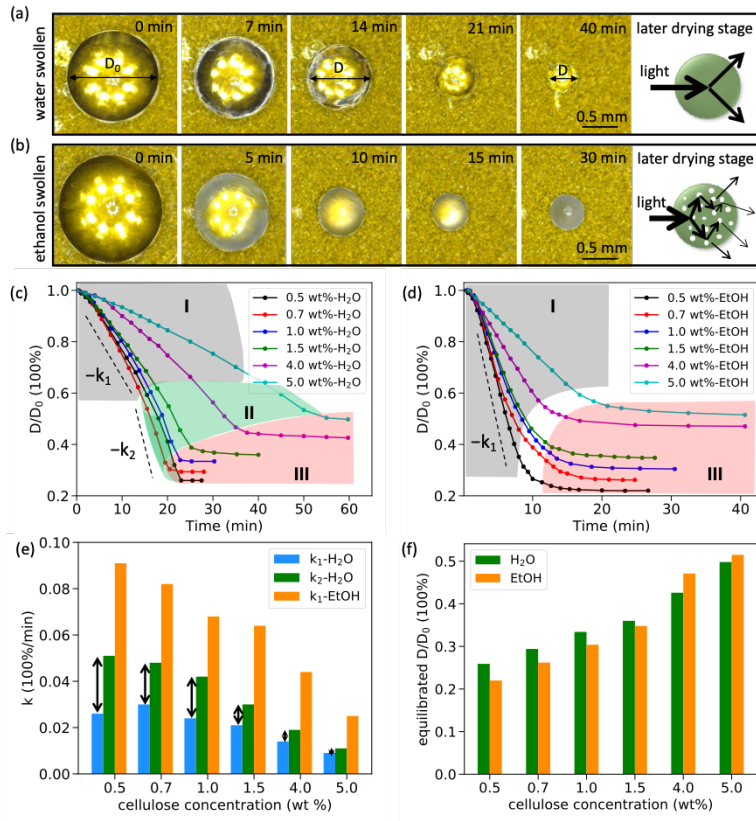
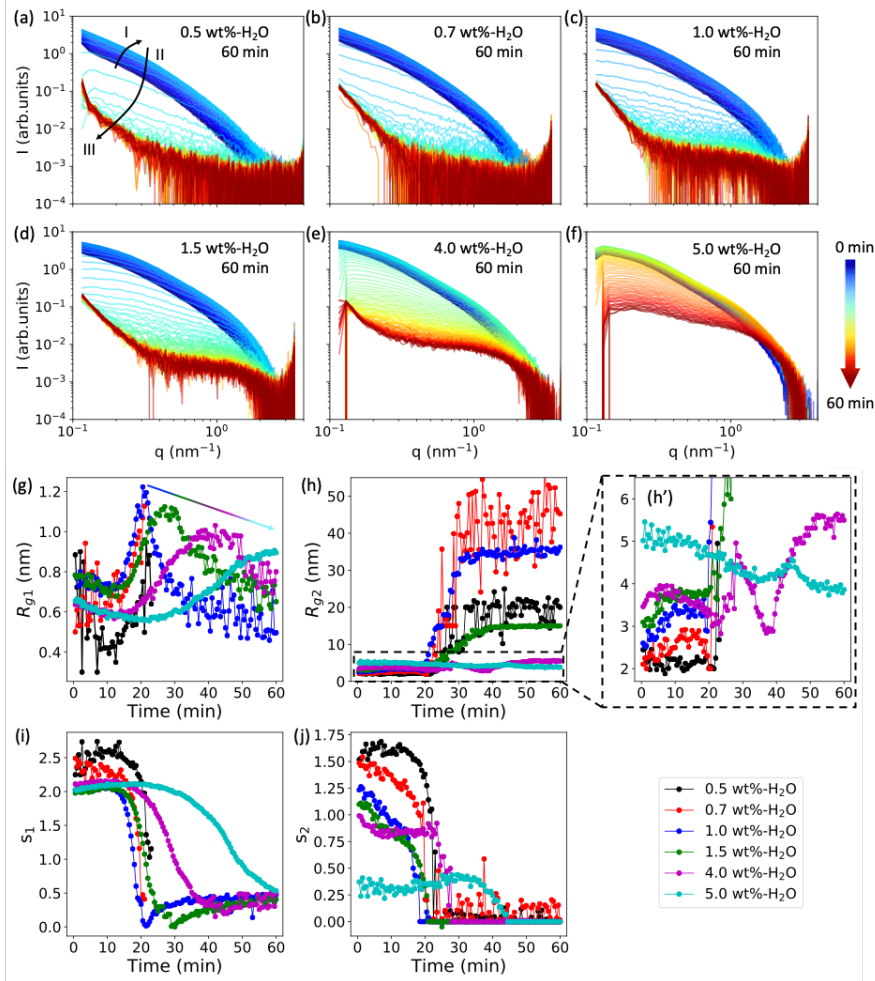


**Figure 3.** Representative top-view optical microscope images of (a) 1.0 wt%-H<sub>2</sub>O and (b) 1.0 wt%-EtOH beads during drying on Kapton tape at 26°C and 33% RH (scale bars are 0.5 mm for all images). The normalized diameter  $D/D_0$  for (c) water swollen and (d) ethanol swollen beads during drying. (e) The linear shrinking rate ( $k_1$  and  $k_2$ ) in drying phases I and II. (f) The equilibrated  $D/D_0$  vs. cellulose concentration for water swollen and ethanol swollen beads.

1     **Structural evolution of gel beads during drying: Small-Angle X-ray Scattering (SAXS).** To  
2     complement the studies of the bead drying on the macroscopic scale; SAXS was used, as depicted  
3     in **Figure S5a**, to study structural changes on the microscale of water swollen and ethanol swollen  
4     beads during drying. Representative 2D SAXS patterns for 1.5 wt%-H<sub>2</sub>O beads are presented in  
5     **Figure S5b**. The homogenous scattering patterns indicate an isotropic structure of the cellulose  
6     gel bead network throughout the drying process, which is consistent with the aforementioned  
7     results that showed the gel bead retaining its spherical shape during drying (Figure 3a, 3c, and  
8     Figure 1b). The scattering intensity increases in the early drying stage (< 20.5 min), then drops to  
9     a significantly lower value over the following two minutes before staying constant.

10    **Figures 4a-4f** show 1D SAXS curves for all water swollen beads throughout the drying process,  
11    achieved through an integration over the full azimuthal angle range of the 2D SAXS patterns.  
12    Similar to the  $D/D_0$  vs. time curves shown in Figure 3c, three regimes can be distinguished in the  
13    SAXS curves for water swollen beads (as indicated by arrows and roman numerals for the different  
14    phases of the 0.5 wt%-H<sub>2</sub>O bead shown in Figure 4a). In regime I, the shape of SAXS curves does  
15    not change significantly, although the intensity increases with evaporation time due to more X-  
16    rays being scattered by objects in the beads during shrinking. After drying for around 20 min  
17    (regime II) the intensity of the SAXS curves decreases rapidly with increasing evaporation time  
18    and the curves start to bend up in the low  $q$  region; which indicates that a potential structural  
19    change is occurring during this time period. In the later drying phase (regime III), the SAXS curves  
20    remain relatively unchanged, and consequently it is assumed that there is no structural change in  
21    the beads in this regime. These three drying regimes were observed in all water swollen beads with  
22    a cellulose concentration of 4.0 wt% or less (Figure 4a-4e). However, for the 5.0 wt%-H<sub>2</sub>O bead

- 1 (Figure 4f), the SAXS curve does not bend upwards in the low  $q$  region in the final drying phase,
- 2 unlike the lower cellulose concentration beads.



3  
4 **Figure 4.** (a-f) SAXS curves for 0.5, 0.7, 1.0, 1.5, 4.0, and 5.0 wt%-H<sub>2</sub>O beads measured during  
5 drying over 60 min, with a time step of 30 seconds between each curve. The color arrow bar  
6 indicates the drying time from 0 min (blue) to 60 min (red). (g-j) The change in the fitted length  
7 scale ( $R_{g1}$  and  $R_{g2}$ ) and 'dimensionality' parameters ( $s_1$  and  $s_2$ ) as a function of the drying time.

1 To quantitatively evaluate the microscale structural changes of the cellulose beads, a Guinier-  
2 Porod model<sup>33</sup> was used to consistently fit the SAXS data collected during the drying process. In  
3 this model, two characteristic length scales ( $R_{g1}$  and  $R_{g2}$ ) and corresponding ‘dimensionality’  
4 parameters ( $s_1$  and  $s_2$ ) are defined to characterize the shape of the objects present within the  
5 system. The fit functions and analysis procedure are summarized in detail in the literature<sup>34,35</sup>, as  
6 well as in our previous work.<sup>25</sup> Briefly,  $R_{g1}$ , in the size range of the anhydroglucose unit, is related  
7 to the local cellulose monomer and  $R_{g2}$  corresponds to the size of the elongated aggregate  
8 structures of the anhydroglucose units inside the gel beads. The shape of the structures can be  
9 determined by  $s_1$  and  $s_2$ : when  $s_1 = s_2 = 0$ , the scattering object has a spherical symmetry; if  
10  $s_1 = 1$  and  $s_2 = 0$ , it has a cylindrical shape; and when  $s_1 = 2$  and  $s_2 = 0$ , it corresponds to a  
11 lamellae structure with equal width and length. However, the real-world microscopic structure of  
12 the cellulose beads is non-ideal and complex, especially during drying, we suggest that it is best  
13 represented by a combination of the aforementioned structures. **Figure S6** shows raw data  
14 measured during the drying of a 1.0 wt%-H<sub>2</sub>O bead and the corresponding fitting curves.

15 Figure 4g-4j summarize the  $R_{g1}$ ,  $R_{g2}$ ,  $s_1$ , and  $s_2$  values of all the water swollen beads throughout  
16 the drying process. As with the macroscopic drying behavior observed in Figure 3c, the evolution  
17 of  $R_{g1}$  values can be divided into three regimes (Figure 4g). For 1.0 wt%-H<sub>2</sub>O swollen beads (blue  
18 curve in Figure 4g), the value of  $R_{g1}$  decreases from 0.78 nm to 0.71 nm during the first 12 min  
19 (regime I) and then quickly increases to 1.2 nm during the next 8 min (regime II), after which it  
20 decreases to 0.6 nm in 15 min before steadily decreasing to 0.5 nm (regime III). For beads with  
21 cellulose concentrations of 1.0 wt% and higher, all the water swollen beads have similar  $R_{g1}$  vs.  
22 time curves with three regimes. The exception to this is the 5.0 wt%-H<sub>2</sub>O beads on which no  
23 regime III was observed due to not practically taking the measurements over a sufficiently long

1 period of time for these samples to dry to this stage. At higher cellulose concentrations, the  $R_{g1}$   
2 vs. time curves are stretched for each regime due to the slower drying rate of these beads. The  
3 maximum value of  $R_{g1}$  decreases from 1.2 nm to 0.9 nm when the cellulose concentration is  
4 increased from 1.0 wt% to 5.0 wt%. In regime III, the  $R_{g1}$  decrease is slower, with a higher value  
5 at 60 minutes for higher concentration cellulose beads. For the 0.5 wt%-H<sub>2</sub>O and 0.7 wt%-H<sub>2</sub>O  
6 beads, similar trends in the curves are observed. However, the SAXS curves are quite noisy in the  
7 high  $q$  region in the later drying phase (regime III in Figure 4a and 4b) and the extracted values  
8 for  $R_{g1}$  and  $s_1$  after a drying time of 22 min are therefore less reliable and are not plotted in Figure  
9 4g and 4i, but have been included for reference in **Figure S7**. As predicted from the  
10 aforementioned  $R_{g1}$  evolution [of gel beads with high cellulose concentrations](#), a much faster  
11 decrease and lower values of  $R_{g1}$  in regime III are observed when beads are made with lower  
12 cellulose concentrations [although the extracted values have slightly large errors](#).

13 The aggregate structure ( $R_{g2}$ ) size in 1.0 wt%-H<sub>2</sub>O beads (blue curve in Figure 4h and 4h')  
14 increases from 2.50 nm to 3.25 nm during the first 12 min of drying (regime I). After which it  
15 remains constant during the next 8 min of drying (regime II), before increasing to 32.00 nm over  
16 the next 15 min, and reaching 36.0 nm after a final 25 min of drying (regime III). Although the  
17 diameter of the gel bead decreases minimally in regime III (see Figure 3c), a sharp increase of  $R_{g2}$   
18 is observed here. Indicating that the nanoscale structures change significantly for 1.0 wt%-H<sub>2</sub>O  
19 beads during the later drying phase. As proposed in our previous work,<sup>25</sup> the rapid increase of  $R_{g2}$   
20 is related to a sharp structural transition caused by the collapse of the nanoporous structure.

21 A similar trend and sharp increase of  $R_{g2}$  vs. time are observed for 0.5, 0.7, 1.5 and 4.0 wt%-  
22 H<sub>2</sub>O beads, while for 5.0 wt%-H<sub>2</sub>O beads there is no sharp increase in  $R_{g2}$ . Figure 4h' shows that  
23  $R_{g2}$  for the 5.0 wt%-H<sub>2</sub>O bead decreases from 5.2 nm to 4.1 nm in the first 35 min before slightly

1 increasing to 4.6 nm over the next 10 min, and finally decreasing to 3.9 nm in the later drying  
2 phase. Interestingly,  $R_{g2}$  shows higher values for increasing cellulose concentrations before drying  
3 (Figure 4h'), but shows lower values for increasing cellulose concentrations after 60 min of drying,  
4 with the exception of the 0.5 wt%-H<sub>2</sub>O bead (Figure 4h).

5 The  $R_{g1}$ ,  $R_{g2}$ , and shape factors indicate that aggregates are formed by entanglements of the  
6 cellulose chains in the presence of non-solvents as they evaporate. The size changes of these  
7 aggregates are illustrated in **Figure 5**. In regime I, the number of entanglements increases with  
8 increasing cellulose concentrations, which leads to the formation of many large aggregates. As a  
9 consequence, the gel beads become much stronger and more resilient to the collapse of the porous  
10 structure. This is observed on the 5.0 wt%-H<sub>2</sub>O bead as an absence of the sharp increase in  $R_{g2}$ .  
11 For the 0.5 wt%-H<sub>2</sub>O bead, the final value of  $R_{g2}$  is about 20 nm, which is smaller than the values  
12 observed for the 0.7 and 1.0 wt%-H<sub>2</sub>O beads. We suggest that the probable reason for this is that  
13 the very low cellulose concentration prevents the formation of aggregates inside the 0.5 wt%-H<sub>2</sub>O  
14 bead. This explanation is consistent with the lower shrinking rate ( $k_1$ ) measured for the 0.5 wt%-  
15 H<sub>2</sub>O bead compared with the 0.7 and 1.0 wt%-H<sub>2</sub>O beads (Figure 3e). Figure 4i shows that the  
16 'dimensionality' parameter  $s_1$  stays in the range of 2.5-2.0 in regime I, quickly decreasing to 0.5  
17 in regime II, and then staying constant at this value in regime III. However, as observed in Figure  
18 4j,  $s_2$  changes at the beginning of the bead drying, from 1.6 for 0.5 wt%-H<sub>2</sub>O beads to 0.3 for 5.0  
19 wt%-H<sub>2</sub>O beads, before quickly decreasing to 0 in regime II and staying at 0 in regime III. The  
20 evolution of  $s_1$  and  $s_2$  suggests that the shape of the aggregates change from elongated to spherical  
21 during the drying process, and the cellulose chains rearrange within low concentration beads into  
22 spherical aggregates with cellulose-II crystalline structures (Discussed further in WAXS section).

Moreover, the initial shapes of the aggregates in regime I are more elongated in beads with higher cellulose concentrations (Figure 5).

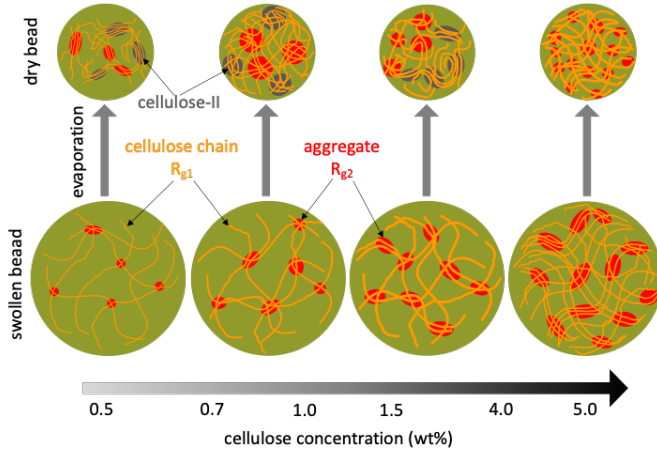


**Figure 5.** Illustration of the structural evolution of water swollen beads during water evaporation from cellulose gel beads with different cellulose concentrations, based on SAXS/WAXS measurements.

The SAXS measurements were also performed on ethanol swollen beads as they dried, and the extracted 1D SAXS curves are shown in **Figure 6a-6f**. The evolution of the SAXS curves for 0.5 wt%-EtOH beads shown in Figure 6a are similar to the ones for the 0.5 wt%-H<sub>2</sub>O beads shown in Figure 4a. However, when the cellulose concentration is 0.7 wt% or higher, the three drying regimes observed for water swollen beads are not observed in ethanol swollen beads (Figure 6b-6f). The shape of the SAXS curves does not vary significantly during the drying process, except for in the early drying phase of the 0.7 wt%-EtOH and 1.0 wt%-EtOH beads. The fitted values of  $R_{g1}$ ,  $R_{g2}$ ,  $s_1$  and  $s_2$  are summarized in Figure 6g-6j. For cellulose concentrations greater than 0.7 wt%,  $R_{g1}$  rapidly decreases from roughly 0.9 nm to approximately 0.6 nm in less than 10 min, after which it remains relatively constant throughout the later drying phase (Figure 6g). A similar



1 trend in  $R_{g2}$  is observed, Figure 6h'. Interestingly, the sharp increase of  $R_{g2}$  observed for water  
2 swollen beads is not seen here (Figure 6h'). Thus, the structure of ethanol swollen beads does not  
3 change significantly, the porous structure does not collapse during the evaporation of ethanol for  
4 beads with cellulose concentrations of 0.7 wt% or greater, which is consistent with our previous  
5 work.<sup>25</sup> From the change of the 'dimensionality' parameters ( $s_1$  and  $s_2$ ) with drying time,  
6 illustrated in Figure 6i and 6j, the shapes of these structures in ethanol swollen beads with cellulose  
7 concentrations of 0.7 wt% and higher are relatively constant when compared to the corresponding  
8 water swollen beads. However, for 0.5 wt%-EtOH beads, the trends in  $R_{g1}$ ,  $R_{g2}$ ,  $s_1$  and  $s_2$  vs. time  
9 (Figure 6h, 6j and **Figure S8**) are similar to those of the 0.5 wt%-H<sub>2</sub>O bead; where a sharp increase  
10 in  $R_{g2}$  is observed. This indicates that the sharp structural change can also occur in the ethanol  
11 swollen bead as long as the cellulose concentration is sufficiently low *e.g.* 0.5 wt%.

12 Based on the SAXS results, we propose an interpretation of the phenomenon observed in Figure  
13 3f, where equilibrated  $D/D_0$  values of 0.5, 0.7, 1.0, and 1.5 wt%-H<sub>2</sub>O beads are larger than the  
14 values of the corresponding ethanol swollen beads. Notably, the equilibrated  $D/D_0$  values of 4.0  
15 and 5.0 wt%-H<sub>2</sub>O beads are lower than those of 4.0 and 5.0 wt%-EtOH beads. Firstly, there is no  
16 structural transition in the 5.0 wt%-H<sub>2</sub>O bead (Figure 4h) or in the 5.0 wt%-EtOH bead. Therefore,  
17 when comparing the drying of the 5.0 wt%-EtOH and 5 wt%-H<sub>2</sub>O beads, structural changes are  
18 ignored. Secondly, from our previous atomic force microscopy (AFM) indentation experiments<sup>32</sup>  
19 we know that the Young's modulus determined in the early drying phase for the water swollen  
20 bead is lower than for an ethanol swollen bead with the same cellulose concentration. This means  
21 that the water swollen bead has a higher tendency to deform in the early drying phase. Thirdly, the  
22 surface tension of water is 72 mN/m, which is three times higher than that of ethanol, 22 mN/m.<sup>36</sup>  
23 Given these three facts, it follows logical intuition that 5.0 wt%-H<sub>2</sub>O beads are more easily

1 deformed than 5.0 wt%-EtOH beads. The same is valid for the 4.0 wt% beads, although the size  
2 of  $R_{g2}$  for 4.0 wt%-H<sub>2</sub>O bead does increase very slightly from 4 nm to 5.5 nm in the later drying  
3 phase (Figure 4h'). Therefore, the equilibrated  $D/D_0$  values of 4.0 and 5.0 wt%-H<sub>2</sub>O beads are  
4 smaller than those of 4.0 and 5.0 wt%-EtOH beads. This situation is reversed for the 0.5, 0.7, 1.0,  
5 and 1.5 wt%-H<sub>2</sub>O beads for which there are rapid structural changes during drying (Figure 4h).  
6 The most probable reason is that the cellulose network structures formed during drying (illustrated  
7 in Figure 5) prevent bead deformation and, as a result, the equilibrated  $D/D_0$  values of 0.5, 0.7,  
8 1.0, and 1.5 wt%-H<sub>2</sub>O beads are larger than those of the 0.5, 0.7, 1.0, and 1.5 wt%-EtOH beads.

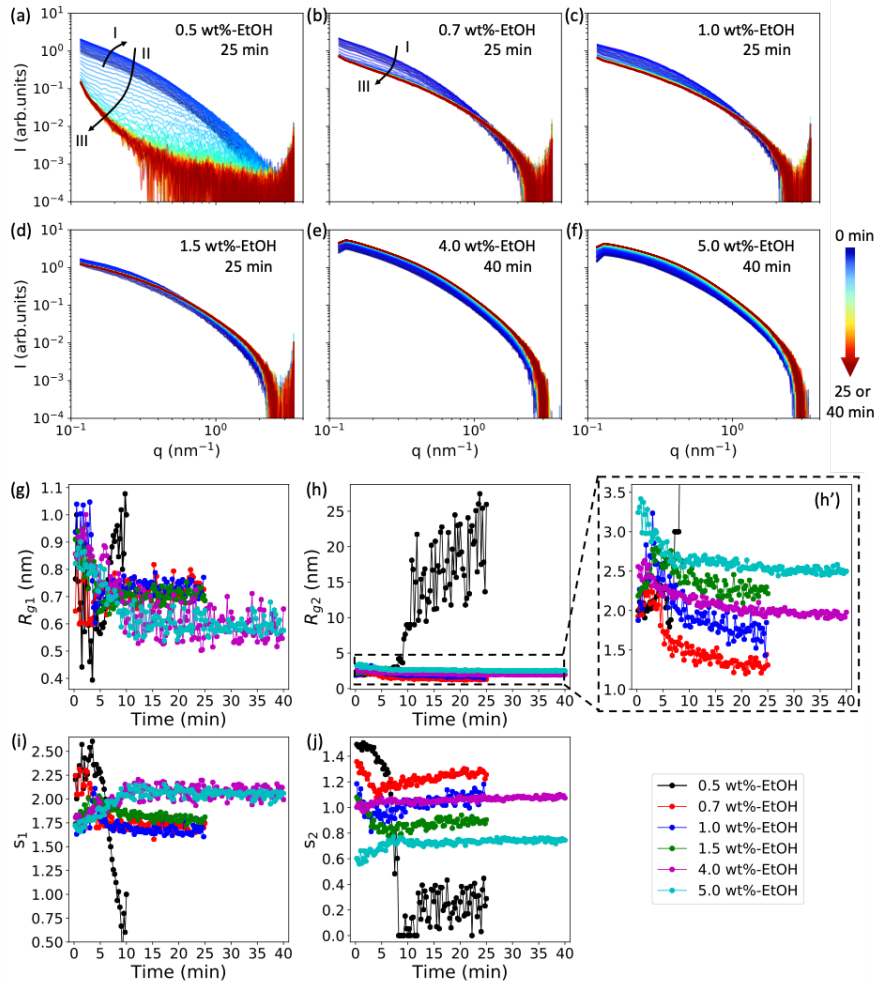


**Figure 6.** (a-f) SAXS curves for 0.5, 0.7, 1.0, 1.5, 4.0, and 5.0 wt%-EtOH beads measured during drying over a time of 25 or 40 min, with a time step of 15 seconds between each curve. The colored arrow bar indicates the drying time from 0 min (blue) to 25 or 40 min (red). (g-j) The change in the fitted length scale ( $R_{g1}$  and  $R_{g2}$ ) and 'dimensionality' parameters ( $s_1$  and  $s_2$ ) as a function of the drying time.

**Wide-Angle X-ray Scattering (WAXS).** To investigate whether any crystalline order is developed during the drying process, WAXS measurements were conducted for 0.5 wt% and 1.5 wt% beads swollen in water and ethanol; the corresponding WAXS curves measured during the drying process are summarized in **Figure 7a-7d**. According to our previous work<sup>25</sup> and the literature<sup>37-40</sup>,  $q = 8.8$  and  $14.6 \text{ nm}^{-1}$  (indicated by magenta arrows in Figure 7a-7c) are assigned to (110) and (110) crystallographic planes of the cellulose II structure.  $q = 20.0$  and  $15.5 \text{ nm}^{-1}$  (indicated by black and red arrows) are assigned to scattering peaks from water and ethanol, respectively.<sup>41,42</sup> For all the beads, no scattering peaks from the cellulose crystalline structure were observed before drying, which indicates that the swollen beads are amorphous. In the early drying phase, the intensity of the scattering peaks from the non-solvents (water or ethanol) decreases quickly, due to evaporation. After this, the scattering peaks from the cellulose II structure appear and their intensity increases with evaporation time for the 0.5 wt%-H<sub>2</sub>O, 1.5 wt%-H<sub>2</sub>O, and 0.5 wt%-EtOH beads. This means that the crystalline structures (cellulose II) are formed in drying phase II and grow as the drying time increases. In the SAXS results a sharp increase of  $R_{g2}$ , which measures the size of the aggregate structures, was also observed for 0.5 wt%-H<sub>2</sub>O, 1.5 wt%-H<sub>2</sub>O, and 0.5 wt%-EtOH beads in drying phase II. Thus, we can correlate these two phenomena and propose that cellulose chains reorganize into larger crystalline aggregates, as illustrated by the grey domains in Figure 5, during the second drying phase. This hypothesis is further evidenced by the fact that there were no cellulose II scattering peaks for the 1.5 wt%-EtOH bead after drying, as would be expected since there was no sharp increase of  $R_{g2}$  observed in the SAXS measurements of the same bead (Figure 6h). This prediction is supported by the result in Figure 7d, where no scattering peaks attributable to cellulose II structure are observed. [According to the aforementioned hypothesis, the formation time and the size of crystalline domains for different gel](#)

beads can be obtained from Figure 4h and Figure 6h. For example, for 0.7 wt%-H<sub>2</sub>O beads, the crystalline domain starts to form after the first 20 min's drying and its size increases to ca. 40 nm in 10 min. While, for 1.5 wt%-H<sub>2</sub>O beads, after the first 20 min's drying the crystalline domain starts to form and its size increases to 20 nm in 20 min. Therefore, the formation time and size of the crystalline domains for different cellulose gel beads are determined by both cellulose concentration and non-solvents. Note, due to the strong scattering of solvents, the solvent fraction during drying, and the difficulty of identifying the amorphous background, it is hard to precisely determine the crystallinity of the drying beads from the present measurements. The orientation of the cellulose-II structure is eliminated due to the spherical shape of the gel beads and their affine shrinkage during drying.

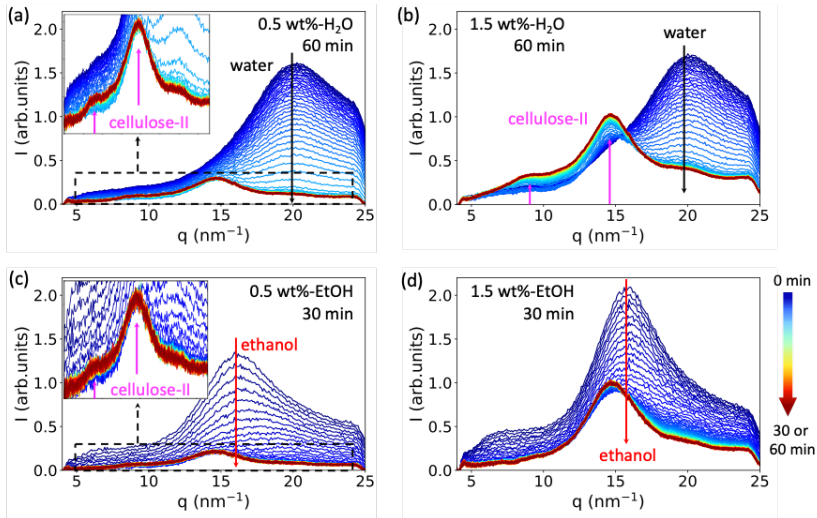


**Figure 7.** WAXS curves for (a) 0.5 wt%-H<sub>2</sub>O, (b) 1.5 wt%-H<sub>2</sub>O (c) 0.5 wt%-EtOH and (d) 1.5 wt%-EtOH beads during the drying process. Water swollen and ethanol swollen beads were dried for 60 min and 30 min, respectively. Each curve was measured at 30 s and 15 s intervals for water swollen and ethanol swollen beads, respectively. The color arrow bar indicates the drying time from 0 min (blue) to 30 min or 60 min (red).

**Non-solvent effect.** To investigate the effect of the non-solvent on the drying behavior, additional SAXS measurements were performed for the 1.5 wt% cellulose gel beads swollen with different water/ethanol mixtures. The extracted 1D SAXS curves for all 1.5 wt% gel beads swollen by water, ethanol and water/ethanol mixtures (volume ratio: 80/20, 60/40, 40/60, and 20/80) during the drying process are shown in **Figure 8a-8f**. Before drying, the SAXS curves for all the beads are very similar, except for the 1.5 wt%-EtOH bead (Figure 8f). The gel beads in Figure 8b-8e show three drying regimes, which are the same as observed in the 1.5 wt%-H<sub>2</sub>O bead (Figure 8a). However, in the very late drying phase the shape of the SAXS curves for these beads changes as the ethanol fraction is increased, especially in the high  $q$  region:  $q > 0.5 \text{ nm}^{-1}$  (from Figure 8b to Figure 8e). In the SAXS results for water swollen beads (Figure 4), it can be seen that there is a sharp structural change for all the 1.5 wt% gel beads swollen with water/ethanol mixtures. This is verified by the fitting results plotted in Figure 8g-8j and **Figure S9**, where a sharp increase in  $R_{g2}$  is observed for all the 1.5 wt% gel beads swollen in water/ethanol mixtures. However, [for the 1.5 wt% gel bead swollen with water/ethanol \(20/80\),  \$R\_{g2}\$  only slightly increases](#) from 2.5 nm to 4.5 nm [meaning that the aggregation size gets roughly two times larger](#). It is significantly lower than for the other water/ethanol mixtures (Figure 8h), most probably due to its low water content. In the case of the 1.5 wt%-EtOH bead, which contains only 4 vol% water,  $R_{g2}$  does not increase during drying. Based on these results, it is suggested that, from a structural point of view, water affects the drying behavior more than ethanol. This is to be expected given the large interaction between water and cellulose.

**hat gelöscht:** the increase of

**hat gelöscht:** for the 1.5 wt% gel bead swollen with water/ethanol (20/80)

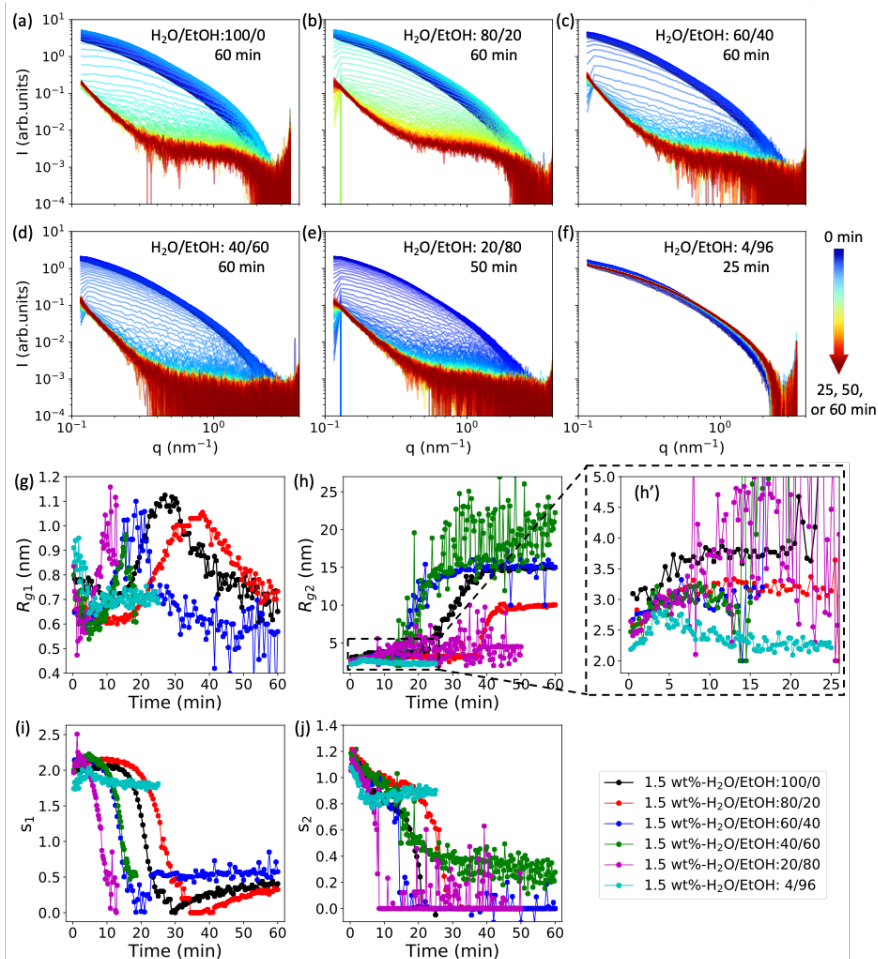


**Figure 8.** SAXS curves measured for 1.5 wt% cellulose gel beads swollen by (a) water, (b-e) different water/ethanol mixtures, and (f) ethanol, during drying process over a time of 60, 50, or 25 min, with a time step between each curve of 30 seconds for (a-c) and 15 seconds for (d-f). The color arrow bar indicates the drying time from 0 min (blue) to 25, 50, or 60 min (red). (g-j) The change in the fitted length scale ( $R_{g1}$  and  $R_{g2}$ ) and 'dimensionality' parameters ( $s_1$  and  $s_2$ ) as a function of the drying time.

hat gelöscht: during drying

Based on the results obtained from SAXS and WAXS measurements, a simplified schematic illustration summarizing the structural evolution of cellulose gel beads [drying from water, ethanol, and water/ethanol mixtures](#) is presented in **Figure 9**. [Note, the applicability of this phase diagram for other non-solvents needs to be further investigated.](#) This phase diagram enables the quick and easy prediction of the drying behavior of regenerated cellulose gel materials swollen by water/ethanol mixtures on the macro- and micro- scale. For example, when the cellulose concentration is lower than 0.5 wt%, there will always be a structural change regardless of the ratio of the water/ethanol mixture used. When the cellulose concentration is higher than 5.0 wt%, there will never be any structural change in any of the samples, regardless of the water/ethanol ratio. However, when the cellulose concentration is between 0.5 wt% and 5.0 wt%, the occurrence of the structural change depends on the non-solvent composition. For example, the structure change can be observed for 1.5 wt% beads when the water fraction in the non-solvent is greater than 20 vol%. [However, more precise phase diagram with accurate phase boundary needs to be updated in the future work.](#)

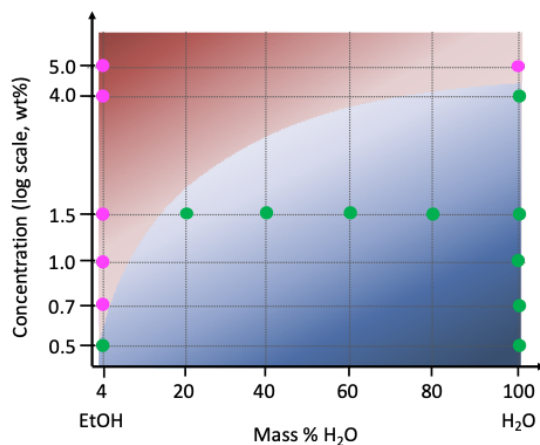




**Figure 9.** A [simplified](#) schematic illustration summarizing the structural evolution during drying of the cellulose beads based on SAXS and WAXS results. Green points represent a three-step drying process in which there is a sharp structural change, and magenta points show a two-step drying process where there is no sharp change in the cellulose structure.

## CONCLUSION

The drying behaviors of regenerated cellulose gel beads with different cellulose concentrations and swollen by water, ethanol or water/ethanol mixtures were investigated. The drying kinetics were traced by *in situ* optical microscopy, SAXS, and WAXS. From the macro scale changes in bead diameter and the micro or nano scale structural evolution during drying; a two-step or a three-step drying process is observed, depending on the cellulose concentration and the non-solvent used. A simplified phase diagram is proposed to describe the cellulose gel beads' drying behavior. When the cellulose concentration is lower than 0.5 wt%, a three-step drying process is observed for all the gel beads studied, regardless the ratio of water to ethanol in the non-solvent used. A sharp structural transition corresponding to the formation of cellulose II crystalline structures occurs during the three-step drying. When the cellulose concentration is higher than 5.0 wt%, a two-step drying behavior is observed, independent of the non-solvent composition, no structural transition occurs in these beads. The drying behavior is more complicated when the cellulose concentration is between 0.5 and 5.0 wt%. Both two-step and three-step drying behaviors can be observed depending on the water content of the non-solvent. For example, for 1.5 wt% gel beads, a three-step drying behavior occurs when the water content is higher than 20 % in the water/ethanol mixture, and a two-step drying behavior is observed when the water content is lower than 20 %. The results presented herein further our understanding of the drying behavior of cellulose on a molecular level. Such advances are invaluable for the preparation of cellulose-based materials, such as fibers, membranes and adhesives. It is also of interest that crystalline cellulose II structures

1 can be developed during drying when the regenerated aggregate structures are able to reorganize  
2 at lower concentrations of the cellulose.

3

## 4 **METHODS AND EXPERIMENTAL SECTION**

5 **Materials.** Domsjö dissolving pulp fibres (Domsjö Fabriker AB, Sweden) is the raw material  
6 used to prepare the cellulose/DMAc/LiCl solutions and gel beads. The fibres from this dissolving  
7 pulp contain 96% glucose.<sup>22,43</sup> Lithium chloride (LiCl, puriss p.a., anhydrous  $\geq 99\%$ ), N,N-  
8 dimethylacetamide (DMAc, puriss p.a.,  $\geq 99.5\%$ ), and ethanol (EtOH, 96 vol%), were purchased  
9 from Sigma-Aldrich. All chemicals were used without further purification.

10 **Preparation of cellulose/LiCl/DMAc solution.** To make the cellulose gel beads,  
11 cellulose/LiCl/DMAc solutions with different cellulose concentrations were first prepared  
12 according to a previously established protocol.<sup>21,22,25,32,44,45</sup> The dissolving grade fibres were pre-  
13 washed with deionized water to remove metal ions and dissolved colloidal substances  
14 (carbohydrates, lignin, and extractives). Water saturated dissolving fibres containing 5.0 g of dry  
15 mass were solvent exchanged with ethanol and then DMAc through multiple washing/filtration  
16 steps. The solvent-exchange was performed over 2 days for each solvent, the solvent being  
17 changed at least twice a day, using 150 mL each time. After the solvent exchange, 100 ml of DMAc  
18 was heated to 105 °C for 20 min in an oil bath and 7 g of LiCl was heated in an oven at 105 °C for  
19 30 min to remove entrapped water. The dehydrated LiCl was added to the heated DMAc and then  
20 allowed to cool to 65 °C at which point the DMAc saturated pulp was added. After stirring  
21 overnight, the 5.0 wt% cellulose/LiCl/DMAc solution was obtained. The same procedure was  
22 performed to prepare 1.5 wt% cellulose/LiCl/DMAc solution. Part of 5.0 wt% solution was diluted  
23 to 4.0 wt% and part of 1.5 wt% solution was diluted to 1.0, 0.7, and 0.5 wt% with DMAc.

**Preparation of cellulose swollen beads.** The 6 different concentrated cellulose/DMAc/LiCl

solutions were precipitated dropwise into non-solvent baths (ethanol, 96 vol%), where the cellulose solution drop solidified into the initial cellulose gel beads, as depicted in Figure S1. The precipitation was performed using an infusion pump (Harvard Apparatus, Holliston, MA, model PHD 2000). The prepared beads were left to equilibrate for 24 h in the ethanol baths. Then, the beads prepared from 5.0, 4.0, 1.0, 0.7, and 0.5 wt% solutions were divided into two fractions: i) beads washed with Milli-Q water and ii) beads washed with ethanol. Both fractions were washed with their respective solvents for at least 7 days to ensure a proper removal of the DMAc/LiCl. Beads obtained by washing with water or ethanol (96 vol%) are labelled water swollen beads (5.0 wt%-H<sub>2</sub>O, 4.0 wt%-H<sub>2</sub>O, 1.0 wt%-H<sub>2</sub>O, 0.7 wt%-H<sub>2</sub>O, and 0.5 wt%-H<sub>2</sub>O) and ethanol swollen beads (5.0 wt%-EtOH, 4.0 wt%-EtOH, 1.0 wt%-EtOH, 0.7 wt%-EtOH, and 0.5 wt%-EtOH), respectively.

For the beads prepared from the 1.5 wt% solution, they were divided into six fractions and washed with Milli-Q water, Milli-Q water/ethanol mixtures (volume ratio: 80/20, 60/40, 40/60, 20/80) or ethanol for at least 7 days. These were labelled as 1.5 wt%-H<sub>2</sub>O, 1.5 wt%-H<sub>2</sub>O/EtOH(80/20), 1.5 wt%-H<sub>2</sub>O/EtOH(60/40), 1.5 wt%-H<sub>2</sub>O/EtOH(40/60), 1.5 wt%-H<sub>2</sub>O/EtOH(20/80), and 1.5 wt%-EtOH.

**Preparation of cellulose dry beads.** In order to observe the morphology of the initial cellulose gel beads with a scanning electron microscope (SEM), ethanol swollen beads were chosen to prepare the dry samples using a critical point drying method (CPD), during which the capillary forces between the vapor, liquid and solid cellulose is theoretically excluded.<sup>46</sup> The ethanol swollen cellulose beads were solvent exchanged to pure ethanol over two days refreshing the solvent three times per day. The beads were then placed in the CPD chamber (Autosamdri-815,

1 Tousimis, USA) and liquid carbon dioxide was injected into the chamber under a pressure of *ca.*  
2 50 bar for solvent exchange from ethanol to CO<sub>2</sub>. The conditions of the chamber were then brought  
3 above the CO<sub>2</sub> critical point, to *ca.* 100 bar and 36 °C, after which the chamber was depressurized  
4 and the CO<sub>2</sub> evaporated.

5 **Field Emission Scanning Electron Microscope (FE-SEM).** The interior morphologies of the  
6 CPD dried cellulose beads were characterized using a S-4800 field emission scanning electron  
7 microscope (FE-SEM) (Hitachi, Tokyo, Japan) operating at high vacuum. CPD dried beads were  
8 cut and glued onto a conductive carbon tape on the sample holder, and then coated with Pt/Pd in a  
9 Cressington 208 HR sputter coater (Cressington Scientific Instruments, Watford, UK) for 20 s to  
10 limit sample charging during imaging.

11 **Optical microscope.** An optical camera (AM7013MZT, Dino-Lite Premier Digital  
12 Microscope) was used to monitor the diameter of the cellulose gel beads throughout the drying  
13 process at 26 °C and 33% RH (the same conditions used in the SAXS/WAXS measurements). In  
14 order to be consistent with SAXS/WAXS measurements, Kapton tape (part number: 42-020-0016)  
15 was used as the substrate for this characterization as well.

16 **Small-angle/Wide-angle X-ray Scattering (SAXS/WAXS).** *In situ* SAXS/WAXS  
17 characterization for drying cellulose gel beads were performed at Forschungszentrum Jülich,  
18 Germany. The X-ray source is a D2-MetalJet (Excillum) with a liquid metal anode operating at 70  
19 kV and 3.57 mA with Ga-K $\alpha$  radiation (wavelength  $\lambda = 0.1314$  nm), providing a brilliant and  
20 narrow beam ( $< 100$   $\mu$ m). The X-ray beam was further focused with a focal length of 55 cm, using  
21 a specially made X-ray optic (Xenocs) to provide a very narrow ( $0.15 \times 0.15$  mm<sup>2</sup>) and intense  
22 beam at the sample position. The scattering data were acquired with a position-sensitive detector  
23 (PILATUS 300K, Dectris) with a pixel size of 172  $\mu$ m. After calibration with silver behenate, the

1 sample-to-detector distances were set to 1107 mm and 152 mm for SAXS and WAXS  
2 measurements, respectively. The cellulose beads were adhered to the Kapton tape surface which  
3 prevents the beads from sliding when the sample holder was placed in the vertical position.  
4 Individual 2D scattering patterns were recorded for water and ethanol swollen beads. The SAXS  
5 scans took 30 seconds each and the WAXS took 15 seconds to scan. After radial integration, the  
6 background scattering of the Kapton tape was scaled and subtracted for each curve to obtain more  
7 accurate data. Scaling was completed to account for the change in X-ray transmission that occurs  
8 from bead shrinking during drying.

9

## 10 **ASSOCIATED CONTENT**

### 11 **Supporting Information**

12 Supporting Information is available free of charge on the ACS Publications website at DOI: (will  
13 be filled in by the editorial staff).

14

## 15 **AUTHOR INFORMATION**

### 16 **Corresponding Author**

17 **Hailong Li** - Department of Fibre and Polymer Technology, KTH Royal Institute of Technology,  
18 Teknikringen 56, SE-100 44 Stockholm, Sweden; Department of Physics, AlbaNova University  
19 Center, Stockholm University, 10691 Stockholm, Sweden; orcid.org/0000-0002-0974-9638;  
20 Email: haili@kth.se

21 **Torbjörn Pettersson** - Department of Fibre and Polymer Technology, KTH Royal Institute of  
22 Technology, Teknikringen 56, SE-100 44 Stockholm, Sweden; Wallenberg Wood Science Centre,  
23 KTH Royal Institute of Technology, Teknikringen 56, 10044 Stockholm, Sweden; orcid.org/0000-  
24 0002-5444-7276; Email: torbj@kth.se

1 **Lars Wågberg** - Department of Fibre and Polymer Technology, KTH Royal Institute of  
2 Technology, Teknikringen 56, SE-100 44 Stockholm, Sweden; Wallenberg Wood Science Centre,  
3 KTH Royal Institute of Technology, Teknikringen 56, 10044 Stockholm, Sweden; orcid.org/0000-  
4 0001-8622-0386; *Email*: wagberg@kth.se

#### 5 **Author**

6 **Margarita Kruteva** - Jülich Centre for Neutron Scattering and Biological Matter (JCNS-1/IBI-  
7 8), Forschungszentrum Jülich GmbH, D-52425 Jülich, Germany; orcid.org/0000-0002-7686-  
8 0934

9 **Martin Dulle** - Jülich Centre for Neutron Scattering and Biological Matter (JCNS-1/IBI-8),  
10 Forschungszentrum Jülich GmbH, D-52425 Jülich, Germany; orcid.org/0000-0001-5699-7530

11 **Zhen Wang** - Department of Fibre and Polymer Technology, KTH Royal Institute of Technology,  
12 Teknikringen 56, SE-100 44 Stockholm, Sweden

13 **Katarzyna Mystek** - Department of Fibre and Polymer Technology, KTH Royal Institute of  
14 Technology, Teknikringen 56, SE-100 44 Stockholm, Sweden; orcid.org/0000-0003-1926-2193

15 **Wenhai Ji** - Deutsches Elektronen-Synchrotron (DESY), Notkestr. 85, 22607 Hamburg,  
16 Germany; orcid.org/0000-0002-1480-2181

#### 17 **Author Contributions**

18 H.L., T.P. and L.W. came up with the original idea of conducting the SAXS/WAXS experiments  
19 of the cellulose gel beads. K.M. prepared the cellulose solution. H.L. prepared the cellulose beads  
20 and conducted the SAXS/WAXS experiments. Z.W. conducted the SEM characterization. H.L.

1 did the SAXS/WAXS data analyzing with the help of M.K., D.M., and W.J.. H.L. wrote the initial  
2 draft of the manuscript; all authors have contributed to finalize the manuscript.

3

#### 4 **ACKNOWLEDGEMENTS**

5 This work was supported by the Government Office of Sweden, Ministry of Enterprise and  
6 Innovation (N2016/03931/IF). L.W. acknowledges the KAW foundation for funding through the  
7 Wallenberg Wood Science Centre at KTH.

8

#### 9 **REFERENCES**

- 10 (1) Moon, R. J.; Martini, A.; Nairn, J.; Simonsen, J.; Youngblood, J. Cellulose Nanomaterials  
11 Review: Structure, Properties and Nanocomposites. *Chem. Soc. Rev.* **2011**, *40*, 3941–3994.
- 12 (2) Wang, S.; Lu, A.; Zhang, L. Recent Advances in Regenerated Cellulose Materials. *Prog.*  
13 *Polym. Sci.* **2016**, *53*, 169–206.
- 14 (3) Li, T.; Chen, C.; Brozena, A. H.; Zhu, J. Y.; Xu, L.; Driemeier, C.; Dai, J.; Rojas, O. J.; Isogai,  
15 A.; Wågberg, L.; Hu, L. Developing Fibrillated Cellulose as a Sustainable Technological Material.  
16 *Nature* **2021**, *590*, 47–56.
- 17 (4) Perepelkin, K. E. Lyocell Fibres Based on Direct Dissolution of Cellulose in N-  
18 Methylmorpholine N-Oxide: Development and Prospects. *Fibre Chem.* **2007**, *39*, 163–172.
- 19 (5) Müller, B.; Gebert-Germ, M.; Russler, A. Viscont HT—the Future of High Performance  
20 Viscose Filaments and Their Textile Applications. *Lenzinger Ber* **2012**, *90*, 64–71.
- 21 (6) Qi, H.; Chang, C.; Zhang, L. Properties and Applications of Biodegradable Transparent and  
22 Photoluminescent Cellulose Films Prepared via a Green Process. *Green Chem.* **2009**, *11*, 177–184.
- 23 (7) Qi, H.; Cai, J.; Zhang, L.; Kuga, S. Properties of Films Composed of Cellulose Nanowhiskers

- 1 and a Cellulose Matrix Regenerated from Alkali/Urea Solution. *Biomacromolecules* **2009**, *10*,  
2 1597–1602.
- 3 (8) Yang, Q.; Fukuzumi, H.; Saito, T.; Isogai, A.; Zhang, L. Transparent Cellulose Films with  
4 High Gas Barrier Properties Fabricated from Aqueous Alkali/Urea Solutions. *Biomacromolecules*  
5 **2011**, *12*, 2766–2771.
- 6 (9) Chang, C.; Zhang, L. Cellulose-Based Hydrogels: Present Status and Application Prospects.  
7 *Carbohydr. Polym.* **2011**, *84*, 40–53.
- 8 (10) Gindl, W.; Emsenhuber, G.; Maier, G.; Keckes, J. Cellulose in Never-Dried Gel Oriented by  
9 an AC Electric Field. *Biomacromolecules* **2009**, *10*, 1315–1318.
- 10 (11) Cai, J.; Kimura, S.; Wada, M.; Kuga, S.; Zhang, L. Cellulose Aerogels from Aqueous Alkali  
11 Hydroxide–Urea Solution. *ChemSusChem Chem. Sustain. Energy Mater.* **2008**, *1*, 149–154.
- 12 (12) Gericke, M.; Trygg, J.; Fardim, P. Functional Cellulose Beads: Preparation, Characterization,  
13 and Applications. *Chem. Rev.* **2013**, *113*, 4812–4836.
- 14 (13) Liebert, T. Cellulose Solvents–Remarkable History, Bright Future. In *Cellulose solvents: for*  
15 *analysis, shaping and chemical modification*; ACS Publications, 2010; pp 3–54.
- 16 (14) Cai, J.; Zhang, L.; Zhou, J.; Qi, H.; Chen, H.; Kondo, T.; Chen, X.; Chu, B. Multifilament  
17 Fibers Based on Dissolution of Cellulose in NaOH/Urea Aqueous Solution: Structure and  
18 Properties. *Adv. Mater.* **2007**, *19*, 821–825.
- 19 (15) McCormick, C. L.; Callais, P. A.; Hutchinson Jr, B. H. Solution Studies of Cellulose in  
20 Lithium Chloride and N, N-Dimethylacetamide. *Macromolecules* **1985**, *18*, 2394–2401.
- 21 (16) Morgenstern, B.; Kammer, H. W.; Berger, W.; Skrabal, P. <sup>7</sup>Li-NMR Study on



- 1 Cellulose/LiCl/NN-dimethylacetamide Solutions. *Acta Polym.* **1992**, *43*, 356–357.
- 2 (17) Zhang, C.; Liu, R.; Xiang, J.; Kang, H.; Liu, Z.; Huang, Y. Dissolution Mechanism of  
3 Cellulose in N,N-Dimethylacetamide/Lithium Chloride: Revisiting through Molecular  
4 Interactions. *J Phys Chem B* **2014**, *118*, 9507–9514.
- 5 (18) Dawsey, T. R.; McCormick, C. L. The Lithium Chloride/Dimethylacetamide Solvent for  
6 Cellulose: A Literature Review. *J. Macromol. Sci. Macromol. Chem. Phys.* **1990**, *30*, 405–440.
- 7 (19) Lindman, B.; Karlström, G.; Stigsson, L. On the Mechanism of Dissolution of Cellulose. *J.*  
8 *Mol. Liq.* **2010**, *156*, 76–81.
- 9 (20) Liu, Y.; Stoeckel, D.; Gordeyeva, K.; Agthe, M.; Schütz, C.; Fall, A. B.; Bergström, L.  
10 Nanoscale Assembly of Cellulose Nanocrystals during Drying and Redispersion. *ACS Macro Lett.*  
11 **2018**, *7*, 172–177.
- 12 (21) Carrick, C.; Pendergraph, S. A.; Wågberg, L. Nanometer Smooth, Macroscopic Spherical  
13 Cellulose Probes for Contact Adhesion Measurements. *ACS Appl. Mater. Interfaces* **2014**, *6*,  
14 20928–20935.
- 15 (22) Karlsson, R.-M. P.; Larsson, P. T.; Yu, S.; Pendergraph, S. A.; Pettersson, T.; Hellwig, J.;  
16 Wågberg, L. Carbohydrate Gel Beads as Model Probes for Quantifying Non-Ionic and Ionic  
17 Contributions behind the Swelling of Delignified Plant Fibers. *J. Colloid Interface Sci.* **2018**, *519*,  
18 119–129.
- 19 (23) Karlsson, R.-M. P.; Larsson, P. T.; Hansson, P.; Wågberg, L. The Thermodynamics of the  
20 Water-Retaining Properties of Cellulose-Based Networks. *Biomacromolecules* **2019**.
- 21 (24) Träger, A.; Klein, G.; Carrick, C.; Pettersson, T.; Johansson, M.; Wågberg, L.; Pendergraph,

- 1 S. A.; Carlmark, A. Macroscopic Cellulose Probes for the Measurement of Polymer Grafted  
2 Surfaces. *Cellulose* **2019**, *26*, 1467–1477.
- 3 (25) Li, H.; Kruteva, M.; Mystek, K.; Dulle, M.; Ji, W.; Pettersson, T.; Wågberg, L. Macro- And  
4 Microstructural Evolution during Drying of Regenerated Cellulose Beads. *ACS Nano* **2020**, *14*,  
5 6774–6784.
- 6 (26) Li, H.; Roth, S. V.; Freychet, G.; Zhernenkov, M.; Asta, N.; Wågberg, L.; Pettersson, T.  
7 Structure Development of the Interphase between Drying Cellulose Materials Revealed by In Situ  
8 Grazing-Incidence Small-Angle X-Ray Scattering. *Biomacromolecules* **2021**.
- 9 (27) Stribeck, N. *X-Ray Scattering of Soft Matter*; Springer Science & Business Media, 2007.
- 10 (28) Ehmman, H. M. A.; Werzer, O.; Pachmajer, S.; Mohan, T.; Amenitsch, H.; Resel, R.;  
11 Kornherr, A.; Stana-Kleinschek, K.; Konturi, E.; Spirk, S. Surface-Sensitive Approach to  
12 Interpreting Supramolecular Rearrangements in Cellulose by Synchrotron Grazing Incidence  
13 Small-Angle X-Ray Scattering. *ACS Macro Lett.* **2015**, *4*, 713–716.
- 14 (29) Jones, A. O. F.; Resel, R.; Schrode, B.; Machado-Charry, E.; Röthel, C.; Kunert, B.;  
15 Salzmann, I.; Konturi, E.; Reishofer, D.; Spirk, S. Structural Order in Cellulose Thin Films  
16 Prepared from a Trimethylsilyl Precursor. *Biomacromolecules* **2019**, *21*, 653–659.
- 17 (30) Ohm, W.; Rothkirch, A.; Pandit, P.; Körstgens, V.; Mueller-Buschbaum, P.; Rojas, R.; Yu,  
18 S.; Brett, C. J.; Söderberg, D. L.; Roth, S. V. Morphological Properties of Airbrush Spray-  
19 Deposited Enzymatic Cellulose Thin Films. *J. Coatings Technol. Res.* **2018**, *15*, 759–769.
- 20 (31) Brett, C. J.; Mittal, N.; Ohm, W.; Gensch, M.; Kreuzer, L. P.; Körstgens, V.; Månsson, M.;  
21 Frielinghaus, H.; Müller-Buschbaum, P.; Söderberg, L. D. Water-Induced Structural

- 1   Rearrangements on the Nanoscale in Ultrathin Nanocellulose Films. *Macromolecules* **2019**, *52*,  
2   4721–4728.
- 3   (32) Li, H.; Mystek, K.; Wågberg, L.; Pettersson, T. Development of Mechanical Properties of  
4   Regenerated Cellulose Beads during Drying as Investigated by Atomic Force Microscopy. *Soft*  
5   *Matter* **2020**, *16*, 6457–6462.
- 6   (33) Hammouda, B. A New Guinier-Porod Model. *J. Appl. Crystallogr.* **2010**, *43*, 716–719.
- 7   (34) Ishii, D.; Tatsumi, D.; Matsumoto, T.; Murata, K.; Hayashi, H.; Yoshitani, H. Investigation  
8   of the Structure of Cellulose in LiCl/DMAc Solution and Its Gelation Behavior by Small-Angle  
9   X-Ray Scattering Measurements. *Macromol. Biosci.* **2006**, *6*, 293–300.
- 10   (35) Aono, H.; Tatsumi, D.; Matsumoto, T. Scaling Analysis of Cotton Cellulose/LiCl·DMAc  
11   Solution Using Light Scattering and Rheological Measurements. *J. Polym. Sci. Part B Polym.*  
12   *Phys.* **2006**, *44*, 2155–2160.
- 13   (36) Khattab, I. S.; Bandarkar, F.; Fakhree, M. A. A.; Jouyban, A. Density, Viscosity, and Surface  
14   Tension of Water+ Ethanol Mixtures from 293 to 323K. *Korean J. Chem. Eng.* **2012**, *29*, 812–  
15   817.
- 16   (37) K Mahadeva, S.; Yeol Yang, S.; Kim, J. Effects of Solvent Systems on Its Structure,  
17   Properties and Electromechanical Behavior of Cellulose Electro-Active Paper. *Curr. Org. Chem.*  
18   **2013**, *17*, 83–88.
- 19   (38) Liu, Z.; Sun, X.; Hao, M.; Huang, C.; Xue, Z.; Mu, T. Preparation and Characterization of  
20   Regenerated Cellulose from Ionic Liquid Using Different Methods. *Carbohydr. Polym.* **2015**, *117*,  
21   99–105.

- 1 (39) Isogai, A.; Usuda, M.; Kato, T.; Uryu, T.; Atalla, R. H. Solid-State CP/MAS Carbon-13 NMR  
2 Study of Cellulose Polymorphs. *Macromolecules* **1989**, *22*, 3168–3172.
- 3 (40) Sèbe, G.; Ham-Pichavant, F.; Ibarboure, E.; Koffi, A. L. C.; Tingaut, P. Supramolecular  
4 Structure Characterization of Cellulose II Nanowhiskers Produced by Acid Hydrolysis of  
5 Cellulose I Substrates. *Biomacromolecules* **2012**, *13*, 570–578.
- 6 (41) Hura, G.; Sorenson, J. M.; Glaeser, R. M.; Head-Gordon, T. A High-Quality x-Ray Scattering  
7 Experiment on Liquid Water at Ambient Conditions. *J. Chem. Phys.* **2000**, *113*, 9140–9148.
- 8 (42) Tomšič, M.; Jamnik, A.; Fritz-Popovski, G.; Glatter, O.; Vlček, L. Structural Properties of  
9 Pure Simple Alcohols from Ethanol, Propanol, Butanol, Pentanol, to Hexanol: Comparing Monte  
10 Carlo Simulations with Experimental SAXS Data. *J. Phys. Chem. B* **2007**, *111*, 1738–1751.
- 11 (43) Larsson, P. T.; Svensson, A.; Wågberg, L. A New, Robust Method for Measuring Average  
12 Fibre Wall Pore Sizes in Cellulose I Rich Plant Fibre Walls. *Cellulose* **2013**, *20*, 623–631.
- 13 (44) Berthold, F.; Gustafsson, K.; Berggren, R.; Sjöholm, E.; Lindström, M. Dissolution of  
14 Softwood Kraft Pulps by Direct Derivatization in Lithium Chloride/N,N-Dimethylacetamide. *J.*  
15 *Appl. Polym. Sci.* **2004**, *94*, 424–431.
- 16 (45) Mystek, K.; Li, H.; Pettersson, T.; Françon, H.; Svagan, A. J.; Larsson, P. A.; Wågberg, L.  
17 Wet-Expandable Capsules Made from Partially Modified Cellulose. *Green Chem.* **2020**, *22*, 4581–  
18 4592.
- 19 (46) Wang, B.; Huang, L. X.; Mujumdar, A. S. Drying of Nanosize Products. *Hankb. Ind. drying*,  
20 *3rd edn. CRC Press. New York* **2007**, 713–727.

1  
2  
3  
4  
5  
6  
7  
8  
9

